Conformation-dependent influences of hydrophobic amino acids in two in-register parallel β-sheet amyloids, an α-synuclein amyloid and a local structural model of PrP^{Sc}

Hiroki Otaki[a,1,*], Yuzuru Taguchi[b,1], Noriyuki Nishida[b]

[a]*Center for Bioinformatics and Molecular Medicine, Graduate School of Biomedical Sciences, Nagasaki University, 1-14 Bunkyo-machi, Nagasaki 852-8521, Japan*

[b]*Division of Cellular and Molecular Biology, Graduate School of Biomedical Sciences, Nagasaki University, 1-12-4 Sakamoto, Nagasaki 852-8523, Japan*

Abstract

Prions are pathogens that consist solely of abnormal isoforms of prion protein (PrP^{Sc}) without any genetic material. Therefore, they depend on purely protein-based mechanisms for diversification and maintenance of the pathogenetic information of prion strains. According to the protein-only hypothesis, the pathogenic properties of prions are determined by conformations of the constituent PrP^{Sc}, and alterations to even a single residue can drastically change the properties when the residue is located at a critical structural position of PrP^{Sc}. Interestingly, differences between polymorphic or species-specific residues responsible for the species/strain barriers are often caused by conservative replacements between hydrophobic amino acids. This implies that subtle differences among hydrophobic amino acids are significant for PrP^{Sc} structures. Specifically how the differences affect the structures is difficult to demonstrate due to the lack of detailed PrP^{Sc} structures. Here, we analyzed the influence of different hydrophobic residues on structures of an in-register parallel β-sheet amyloid of α-synuclein (αSyn) using molecular dynamics (MD) simulation, and applied the knowledge from the αSyn amyloid to design local structures of human PrP^{Sc} encompassing residues 107–143. The MD simulations of the αSyn amyloid revealed that methionine uniquely stabilized a U-shaped β-arch of the αSyn amyloid, whereas other hydrophobic amino acids destabilized the β-arch. Then, we assessed influence of the polymorphisms on the newly-designed model of PrP^{Sc} that are known to affect the clinical phenotypes of prion diseases. The MD simulations of the model also revealed unique effects of hydrophobic amino acids depending on regional structures. For example, G127V mutation that corresponds to a protective polymorphism against various human prion diseases greatly destabilized a U-shaped β-arch. Our study demonstrates specifically how and in what structures hydrophobic residues can exert unique effects on in-register parallel β-sheet amyloids and provides insights into the molecular mechanism of the strain diversity of prions and other pathogenic amyloids.

Keywords: prion, prion strain, prion protein, amyloid, in-register parallel β-sheet amyloid, α-synuclein, molecular dynamics simulation, hydrophobic interaction, species barrier, PrP^{Sc}, conformation, β-arch

Author Summary

Prions are unconventional pathogens that encode the pathogenic information in conformations of the constituent abnormal isoform of prion protein (PrP^{Sc}), independently of nucleotide genome. Therefore, conformational diversity of PrP^{Sc} underlies existence of many prion strains and species barriers of prions, although the conformations still remain undetermined. As prion/PrP^{Sc} propagates through refolding the host-encoded prion protein (PrP^{C}) into the same conformation as itself, species barriers occur when the conformation of PrP^{Sc} is incompatible with the amino acid sequence of PrP^{C} and the nascent PrP^{Sc} cannot stably maintain the structure. Interestingly, species barriers are often caused by a difference of a single hydrophobic residue. We investigated how the subtle differences between hydrophobic amino acids affect the structural stabilities of amyloids using molecular dynamics (MD) simulation of a newly designed local structural model of PrP^{Sc}, assuming that it has in-register parallel β-sheet structures. We have found that mutations equivalent to polymorphisms that cause barriers substantially affects the stabilities; for example, G127V mutation that makes the host resistant to various human prion diseases greatly destabilized the amyloid. The results support that PrP^{Sc} is an in-register parallel β-sheet amyloid and demonstrate the usefulness of MD simulation in investigation of species barriers of prions.

1. Introduction

Prion diseases are a group of neurodegenerative disorders that are characterized by the accumulation of the abnormal isoform (PrP^{Sc}) of prion protein (PrP) in the central nervous system [1]. Prion diseases have three etiologies, sporadic, inherited, and acquired, depending on how the causative PrP^{Sc} propagation is initiated in the body. In sporadic and inherited prion diseases, *e.g.*, sporadic Creutzfeldt-Jakob disease (CJD) and fatal familial insomnia (FFI), respectively, the causative PrP^{Sc} are generated by the spontaneous conformational conversion of endogenous normal isoform PrP (PrP^{C}) into PrP^{Sc}, with or without the aid of pathogenic mutations in the *PRNP* gene. Acquired prion diseases are caused by the intake of exogenous PrP^{Sc} as infectious prion agents, such as epidemic bovine spongiform encephalopathy (BSE) in cattle [2] and chronic wasting disease (CWD) in cervids [3]. Prions behave similarly to viruses, with high infectivity, the existence of many strains, species/strain barriers, and adaptation to new hosts, despite the lack of conventional genetic material. These virus-like pathogenic properties of prions are hypothesized to be enciphered in the conformations of PrP^{Sc}, *i.e.*, protein-only hypothesis [1, 4].

Indeed, the pathogenic properties of prions and the consequent clinical phenotypes are greatly affected by the primary structure of constituent PrP^{Sc}, which is consistent with the fundamental fact that conformations of proteins are determined by the primary structures. For example, in sporadic CJD, PrP deposition patterns, lesion profiles in the brain, clinical presentations, and the apparent molecular sizes of protease-resistant cores of PrP^{Sc} vary depending

*Corresponding author

Email addresses: otaki@nagasaki-u.ac.jp (Hiroki Otaki), ytaguchi@nagasaki-u.ac.jp (Yuzuru Taguchi), noribaci@nagasaki-u.ac.jp (Noriyuki Nishida)

[1]The two authors equally contributed to the work.

on whether the polymorphic codon 129 is methionine (M129) or valine (V129) [5]. A pathogenic mutation D178N of human PrP causes either FFI or familial CJD in association with M129 or V129, respectively [6]. The vast majority of new-variant CJD cases, which resulted from the trans-species transmission of BSE to humans, have been homozygous for M129 [7, 8]. Furthermore, the methionine/leucine polymorphism at codon 132 of elk PrP, which is equivalent to the codon 129 polymorphism of human PrP, also affects the susceptibility to CWD [9, 10]. From the viewpoint of the protein-only hypothesis, polymorphisms should affect disease susceptibility through structural alterations of the constituent PrP^{Sc}; however, specifically how the subtle differences between those hydrophobic amino acids affect structures of the PrP^{Sc} has not been identified yet. Detailed structures of PrP^{Sc} are necessary for the investigation, but with all currently available data, even whether PrP^{Sc} is an in-register parallel β-sheet amyloid or a β-solenoid is still controversial due to its incompatibility with conventional high-resolution structural analyses [11–16].

Not only by the methionine/valine polymorphic codon 129, strain/species barriers of prions can be also caused by conservative replacements between different hydrophobic amino acids at other residues. In experiments with a C-terminally-truncated Y145Stop mutant of human PrP and the counterparts of mouse and Syrian hamster PrPs, whether residue 138 or 139 (in human numbering throughout, unless otherwise noted) was isoleucine or methionine was critical for efficient amyloid formation and cross-seeding among them [17, 18]. In the transmission of the prions of sporadic CJD homozygous for M129 to transgenic mice expressing human-mouse chimeric PrP, I138M substitution substantially extended the incubation periods [19]. Different hydrophobic amino acids at codons 109 and 112 influenced the transmission efficiencies of prions among different hamster species [20, 21]. In an experiment observing the influences of systematically-introduced mutations of mouse PrP on the conversion efficiencies in scrapie-infected Neuro2a cells, methionine at some positions, *e.g.*, M213, was replaceable with other hydrophobic residues like leucine without affecting the conversion efficiency, whereas irreplaceable at other residues, *e.g.*, M206 [22]. In *in-vitro* cross-seeding between ovine PrP and cervine CWD, an I208M (in ovine numbering) mutation showed profound influences on seeding efficiencies [23]. Given those documented facts, we are interested in the effect of different hydrophobic residues on structures of in-register parallel β-sheet amyloids, particularly whether methionine has unique properties compared with other hydrophobic amino acids. We thus used an in-register parallel β-sheet amyloid of α-synuclein (αSyn) as a surrogate structural model for PrP^{Sc}, as in our previous studies [24, 25].

αSyn amyloid is the main component of Lewy bodies, which is a hallmark of Parkinson's disease and dementia with Lewy bodies (DLB), and reportedly has prion-like properties which include transmissibility and strain diversity [26]. For instance, αSyn forms various types of amyloids *in vitro*, which are different in appearance, proteolytic fragment patterns, and cytotoxicity [27]. Moreover, αSyn amyloids isolated from DLB and multiple system atrophy had different proteolytic fragment patterns suggestive of distinct conformations [28]. Those findings are highly reminiscent of prions and imply that prion-like properties are inherent in in-register parallel β-sheet structures. Detailed structures of αSyn amyloids have been determined with solid-state NMR (ssNMR) [29] or cryo-electron microscopy [30, 31]; thus we used a Greek-key αSyn amyloid (PDB ID: 2N0A [29], Figure 1A) to investigate the effects of different hydrophobic residues on the in-register parallel β-sheet structures. Our studies have revealed that the

lengths and C_β-branching of the side chains of hydrophobic residues are important for the stability of local amyloid structures, particularly in a U-shaped β-arch. Then, we applied the knowledge from the αSyn amyloid to a local structural model of PrP^{Sc} encompassing residues 107 to 143 of human PrP, $PrP_{107\text{-}143}$, assuming that PrP^{Sc} was also an in-register parallel β-sheet amyloid. We assessed how mutations and polymorphisms associated with the strain diversity of prions affected structures of the model amyloid using molecular dynamics (MD) simulation. Our studies have demonstrated specifically how different types of hydrophobic amino acids affects the structures of in-register parallel β-sheet amyloids of αSyn and $PrP_{107\text{-}143}$. We have also found that the structural stability of U-shaped β-arches requires hydrophobic cores with well-balanced interactions among the constituent hydrophobic residues. Knowledge from the present study will advance our understanding of the strain diversity of amyloids and facilitate designing more plausible PrP^{Sc} models and other amyloids in the future.

2. Results and Discussion

2.1. Investigation of the mechanism of how the G84M mutation stabilizes the αSyn amyloid

To compare the influences of hydrophobic amino acids on the local structures of αSyn amyloids, we introduced methionine substitutions at residues 61 (E61M) and 84 (G84M), where we previously investigated influences of isoleucine substitutions [24]. Figure 1B shows the final snapshots of MD simulations of αSyn amyloids, and Figure 1C shows the heatmaps of the β-sheet propensity. The MD simulations of homo-oligomer amyloids of αSyn(E61M) and αSyn(G84M) revealed that both the mutations tended to stabilize the local structures, particularly when these amyloids induced new β-sheets in the nearby loops encompassing residues 57 to 62 (loop(57–62)) for the E61M mutant, or residues 84 to 87 (loop(84–87)) for the G84M mutant (Figure 1B). In the E61M mutant, the induction of β-sheets in loop(57–62) was mainly in chains C–H, unlike E61I-induced β-sheet, which were mainly on the chain-A side [24]. The effects of the G84M substitution were more impressive. Almost the entire region C-terminal to residue 80, including loop(84–87), converted to stable β-sheets, in contrast to those of G84I substitution [24]. In the G84L mutant, αSyn(G84L), the loop region around L84 was substantially destabilized like that of αSyn(G84I) [24]. A G84V mutant (αSyn(G84V)) also shows similar β-sheet propensity to αSyn(G84L). Being interested in the opposite effects of G84M and G84L/V/I, we focus on residue 84 to identify the underlying mechanisms.

Directions of the side chains of αSyn(G84M) and αSyn(G84L) are compared in the insets of Figure 1B. The final status of 400-ns simulations was different between the αSyn(G84M) and αSyn(G84L) amyloids. All the side chains of methionine at residue 84 (M84) pointed inward of loop(84–87), whereas some side-chains of leucine at residue 84 (L84) flipped and pointed outward.

Hydrophobic contact diagrams are shown in Figure 2. The diagrams of the αSyn(G84M), αSyn(G84L), αSyn(G84V), and αSyn(G84I) amyloids clearly exhibited differences. M84 of αSyn(G84M) amyloid had intra-chain interactions evenly with residues 82 and 89 of the same chain in all the layers, and the interactions were reproducible. In contrast,

αSyn(G84L) and αSyn(G84V) amyloids only infrequently showed that pattern or were similar to those of another destabilizing mutation, G84I [24].

The unique stabilizing effects of M84 would be attributable to the long side-chain, which can extend across the β-arch like a crossbeam. During the simulation, the ends of the side chains were fixed in the proximity of A89 (Movie S1). The intimate interactions with A89 reinforced the hydrophobic core and stabilized the β-arch. Leucine could not replace methionine despite their similarity in hydrophobicity and non-branching C_β atom, because its side chain is not long enough for stable interactions with A89. Even in reality, the subtle difference between methionine and leucine is significant in certain cases of prion propagation, as the methionine/leucine polymorphism of elk PrP affects the susceptibility to CWD infection [9, 10]. The local structures of CWD-PrP^{Sc} around the polymorphic residue might be similar to the U-shaped loop of αSyn, *i.e.*, the long side-chain of methionine is essential for stability.

2.2. Modeling a local structure of PrP^{Sc} based on knowledge from the αSyn amyloids

Given the knowledge from our studies on αSyn amyloids [24, 25], we attempted to model a local structure of PrP^{Sc} with a U-shaped loop. A region comprising a glycine-rich motif encompassing 123–127 of human PrP ($-GGL_{125}GG-$) seems to be suitable for a U-shaped loop. In addition, the anti-prion effect of valine at residue 127 against various sporadic CJD [32] is reminiscent of the destabilizing effects of V84 in the αSyn amyloid, which suggests the presence of a U-shaped loop in the region. Moreover, structures of amyloid cores of Y145Stop-mutant PrP investigated with ssNMR are available, although not in atomic resolution [16, 33]. Amyloids of the Y145Stop-mutant induced infectious PrP^{Sc} that caused *bona fide* prion disease when inoculated into mice [34], and could therefore share similar local structures with full-length PrP^{Sc}. We thus tentatively modeled local structures of PrP^{Sc} in region 107–143, $PrP_{107\text{-}143}$, utilizing the structural model of the Y145Stop mutant propounded by Theint *et al.* [33] and the knowledge from the αSyn amyloid for stable β-arches (Figure 3A). The model amyloid of wild-type (WT) was sufficiently stable in 10-ns MD simulations (Figure 3B, see also Movie S2). We then modeled mutants of $PrP_{107\text{-}143}$ (G127V, M129V, I138M, M129V&I138M, and A133V) and performed MD simulations. The results are discussed in the following sections.

2.3. Influence of G127V mutation on the $PrP_{107\text{-}143}$ amyloid

Final snapshots of MD simulation for G127V mutant, $PrP_{107\text{-}143}$(G127V), are presented in Figure 3C, from which we confirmed the destabilizing effects of the mutation on the U-shaped loop (residues 120–130, see also Movie S3). These effects are reflected in the β-sheet propensity values shown in Figure 4: heatmaps of $PrP_{107\text{-}143}$(G127V) indicate the disorder around the U-shaped loop. To validate the (in)stability, we used proximity scores, which represents the sum total of the persistence of the hydrophobic contacts between two hydrophobic residues over the 10 chains, A–J (Figure S1A). The scores correlated with distances between the two corresponding residues in certain cases (Figure S1B) and reflected the stability of the hydrophobic cores. Figures 5 and 6 summarize the proximity scores

in the U-shaped loop and the N-/C-terminal-side regions, respectively. The proximity scores for V122-M129, L125-L125, and L130-L130 of $PrP_{107\text{-}143}$(G127V) significantly decreased compared with those of the WT. The proximity score for V122-V122 also decreased, although not statistically significant. These results indicate that those residues are frequently wide apart, consistent with disordered U-shaped loops. In the other regions, the proximity scores for A115-V121, A118-A133, and A118-P137 decreased, although not statistically significant. Destabilization of the amyloid structure caused by the G127V mutation is consistent with the protective effects of a V127 polymorphism of human PrP against CJD transmission [32] because the destabilization would abolish propagation of the PrP^{Sc} in the brain.

2.4. Influence of M129V mutation on the $PrP_{107\text{-}143}$ amyloid

Next, we analyzed the influence of M129V substitution, which is equivalent to V129 polymorphism of human PrP, on the stability of the hydrophobic cores. The mutant amyloid, $PrP_{107\text{-}143}$(M129V), appeared more stable during the 10-ns simulation than the WT (Figure 3D). Comparison of their β-sheet propensity values validated the stability, with more demarcated loops (residues 116–119) and smaller standard deviation (SD-β) values in the 129–134 region (Figure 4, compare WT and M129V).

Proximity scores of the WT and the mutant revealed more detailed differences. Most notable was the alteration in the balance of interactions between A120, V122, L125, and V129 in the hydrophobic cores of the U-shaped loops (Figure 5). The WT showed outstandingly high proximity scores for V122-M129 ($\sim$ 650) in the U-shaped loop, whereas the M129V mutation reduced the score and, instead, increased scores for A120-V129 and V122-L125, making the three scores almost equal ($\sim$ 400). Higher scores for A120-A120 and V129-V129 reflected more structural stability of the mutant amyloid. The mutation also affected interactions in remote regions, as demonstrated by significant decreases of the proximity scores for A115-V121 and A118-P137 (Figure 6). Some increases of the proximity scores are also seen, *e.g.*, A113-V121, A117-I139, A118-A133, and I139-I139, although they are not statistically significant. The altered interactions in the N-terminal-side region (A113-V121 and A115-V121) are particularly interesting, because they are located on the other side from V129 across β-strand 120–122 and do not directly contact V129. Presumably, the dynamics of the β-sheet(120–122) were initially affected by the mutation, subsequently altering the interaction patterns of V121.

As shown in Figure 3D, the distance between β-sheet(120–122) and β-sheet(128–133) seems to be narrower in the M129V mutant. Indeed, the M129V mutation increased the proximity scores for A118-A133 (Figure 6), and distances between the C_α atoms of A118 and S132, dC_α(A118–S132), tended to be shorter in mutants with M129V mutations (Figure 7A, green and blue squares) than in WT (red dots). Interestingly, the WT and mutants with M129 mostly had shorter dC_α(A118–A/V133) than dC_α(A118–S132), whereas the two distances of the V129 mutants (M129V and M129V&I138M) were comparable (Figure 7B). Figure 7C presents a correlation between dC_α(A120–M/V129) and dC_α(A118–S132). The mutants with V129 showed obviously shorter dC_α(A120–M/V129) than those with M129. Additionally, in the mutants with V129, the distances between C_α atoms of A120 and V129, dC_α(A120–V129), are

shorter than dC$_\alpha$(V122–V129); while the others show opposite tendency (Figure 7D). All those findings are explainable by assuming the "upward" positional shift of the β-sheet(128–133) in the mutants with V129 (Figure 7E,F) that is attributed to the shorter side-chain of V129 than that of M129. The shortness enabled V129 to further approach toward A120 and consequently caused well-balanced interactions of the hydrophobic residues and closer positioning of the two β-sheets. Besides the local effects, the positional shift also expanded the range of motion of the C-terminal-side region, leading to significant loss of interaction for A118-P137 and facilitating interactions of A116-I139, A116-F141 and A117-I139, although the incremental changes in the proximity scores are not statistically significant (Figure 6). In contrast, with the long side-chain of M129, biased interactions with V122 seem to hamper the approach of residue 129 toward A120 (Figure 5).

2.5. Influence of I138M mutation on the PrP$_{107\text{-}143}$ amyloid with or without M129V mutation

Residue 138 is one of the residues that are often varied between species, *e.g.*, isoleucine in human, methionine in many rodents, and leucine in many ruminants. This residue is the most influential on the mouse-human species barrier in the transmission of sporadic CJD [19] and also in the cross-seeding of Y145Stop peptides of human and mouse PrP [18]. We assessed how the I138M mutation affected the local structural model of PrP^{Sc}. The most remarkable finding is the tendency of the C-terminal-side region to lean over toward the N-terminal-side region (Figure 3E), presumably due to bending at the loop(134–137). Because of the bending, the angle between the β-sheet(128–133) and the β-sheet(139–141) appeared to be near-square to acute in many runs of the I138M mutants, particularly in PrP$_{107\text{-}143}$(M129V&I138M), whereas the WT or other mutants tended to have obtuse angles (Figures 3 and S2).

In a comparison between the I138M mutants and the WT, the β-sheet propensity and the proximity scores are similar but interestingly the proximity scores for A133-P137 are higher in the I138M mutants (Figures 4, 5, and 6) . Figure 8 represents the proximity scores for A133-P137 of each MD run. In the runs with relatively high proximity scores for A133-P137, the amyloids tended to form small loops like an Ω-shape (Figure 3F). This loop is encompassing A133 and P137 and has near-square to acute angles between the β-sheet(128–133) and the β-sheet(139–141), irrespective of the primary structures (see boxed snapshots in Figure S2). The final snapshot of Run 7 of PrP$_{107\text{-}143}$(M129V) (Figure 3D), which has an Ω-shaped loop in the loop(134–137), also had high proximity score (Figure 8).

The deeper bending of the loop, even to acute angles caused by the I138M mutation, would be attributable to the high intrinsic α-helix propensity of methionine [35, 36] to increase the freedom of motion of the loop and the contact of A133 and P137, which is thermodynamically favorable. In this particular conformation, V129 seems compatible with M138, *i.e.*, the "upward shift" of the β-sheet(128–133) brings A133 to a position where P137 can efficiently interact and allows loop(134–137) to bend deeper, without the C-terminal-side region colliding against loop(116–118) (Figures 3A and 7F); as a result, the interaction of A118-P137 is significantly weakened (Figure 6). In contrast, in those with M129, the full extent of deeper bending is not allowed due to steric clash. That may explain why the effects of the I138M mutation were more accentuated in PrP$_{107\text{-}143}$(M129V&I138M) than in PrP$_{107\text{-}143}$(I138M). For example,

a significant difference of the proximity score in A120-M/V129 was observed only between amyloids with V129, *i.e.*, $PrP_{107\text{-}143}$(M129V) and $PrP_{107\text{-}143}$(M129V&I138M) (Figure 5). Possibly, efficient bending of loop(134–137) in $PrP_{107\text{-}143}$(M129V&I138M) may facilitate further shifting of β-sheet(128–133) to cause the difference, whereas the bending tended to be hampered by M129 in $PrP_{107\text{-}143}$(I138M) and the effects of M138 could not be fully manifested. The same explanation holds for the different proximity scores for A116-I139 and A117-A133 (Figure 6).

2.6. Influence of A133V mutation on the $PrP_{107\text{-}143}$ amyloid

V136 (in ovine numbering) is one of scrapie-prone polymorphisms of ovine PrP [37]. In the present model shown in Figure 3A, the corresponding residue of human PrP, A133, faces the same direction as M129; we were therefore interested in whether an A133V mutation somehow affect the $PrP_{107\text{-}143}$ amyloid structures. The mutant $PrP_{107\text{-}143}$(A133V) appeared to have β-sheet(120–122) and β-sheet(128–133) slightly wider apart than the WT and similarly stable as the WT overall (Figures 3G and S2), as confirmed by the similar heatmap patterns (except for a more demarcated loop(116–119)) (Figure 4). Consistent with the appearance, the distances between the C_α atoms of residues 118 and 133 were very stably maintained at $\sim$ 7 Å (Figure 9), with higher proximity score for A118-V133 than that of WT (Figure 6). The interaction of A118-V133 may cause the significant increase of the proximity scores for L130-L130 and M134-M134. In the U-shaped loop, the score for V122-M129 was higher and reciprocally lower for A120-M129 in the A133V mutant than those in the WT, although the differences are not statistically significant. (Figure 5). The proximity scores of interactions in the N-/C-terminal-side regions were also altered: The score for A117-I139 was increased, along with a decrease in the score for A116-I139 (Figure 6). Those alterations could be explained from the viewpoint of the positional relationship between β-sheet(120–122) and β-sheet(128–133), as discussed above (Figure 7E,F). In the A133V mutant, the stable A118-V133 relationship and the stacking interactions of L130 and M134 would fix the positional relationship of the two β-sheets as in the left panel of Figure 7F. This positional relationship would facilitate V122-M129 interaction and keep I139 away from A116 due to the restricted motion range of the C-terminal-side region. The altered balance of the hydrophobic interactions induced by the A133V mutation did not improve the stability of the amyloid as much as the M129V mutation, despite the stabilized relationships of the two β-sheets; thus, simulations of the present model did not provide any clues to the mechanism of how V136 of ovine PrP facilitates conversion to disease.

2.7. Conclusion about the $PrP_{107\text{-}143}$ amyloid model

Collectively, the present local structural model of PrP^{Sc} seems to be more compatible with V129 than with M129. This is an example of an amyloid conformation where differences between methionine and valine affect the structural stability. Another model, which is more compatible with M129 than with V129, is underway.

Reinforcement of a single hydrophobic interaction between the β-sheets induced by mutations, *e.g.*, V122-M129 interaction in $PrP_{107\text{-}143}$(A133V) or A120-V129 interaction in $PrP_{107\text{-}143}$(M129V&I138M) amyloids, did not facilitate the stabilization of the local structures. To the contrary, the significantly lowered L125-L125 proximity score of

$PrP_{107\text{-}143}$(M129V&I138M) suggests that this alteration causes a certain degree of destabilization of the β-arch. The results of αSyn(G84M) and $PrP_{107\text{-}143}$(M129V) imply that well-balanced interactions of constituent residues in the hydrophobic core might be essential for maximal stability of a β-arch.

Incidentally, the spontaneous approach of N- and C-termini of the $PrP_{107\text{-}143}$ amyloid, which occurred with high A/V133-P137 proximity scores, was notable because the N- and C-termini lead to positive- and negative-charge clusters, respectively, in a full-length human PrP. Those charged clusters could electrostatically interact and contribute to the stabilization of the amyloid structures. Interestingly, the positive-charge cluster seemed essential for the structural conversion of the N-terminal region [38].

Knowledge from the present study may help design more plausible PrP^{Sc} models, local structural models of other regions of PrP^{Sc}, and other in-register parallel amyloids. For example, the region between the first and the second α-helices of PrP (residues 155–177), which is likely an interface between substrate PrP^{C} and template PrP^{Sc} on the C-terminal side [39], may also form a β-arch. Conversion efficiencies of mouse PrP into PrP^{Sc} of RML/Chandler scrapie obtained from disulfide-crosslink scanning experiment suggests that side chains of residues 165 and 166 (in mouse PrP numbering) are directed outward from a β-arch, forming a loop [40]; this supports our view. However, because hydrophobic residues are sparse but instead there are many asparagine residues in the region, hydrogen bonds might be more important for reinforcement of the β-arch, rather than hydrophobic effects.

2.8. Potentially generally applicable knowledge from the present study

The unique effects of each group of hydrophobic amino acids in the in-register parallel β-sheet amyloids were conformation-dependent and attributable to C_β-branching and/or length of the side chains. Methionine and isoleucine showed similar influences in a flat-loop of the αSyn amyloid, whereas isoleucine and valine in U-shaped loops destabilized the structures when they were not stably incorporated in hydrophobic cores. As the latter effects were observed in two different proteins, αSyn(G84I) and $PrP_{107\text{-}143}$(G127V), this notion may be generally applicable to other in-register parallel amyloids. In certain situations, methionine can behave distinctly from other hydrophobic amino acids, as in αSyn(G84M) amyloid where its long side-chain stabilized the β-arch as a crossbeam across the arch forming a well-balanced interaction network. The long hydrophobic side-chain of methionine would also be advantageous for efficient inter-domain and intermolecular interactions, as seen in an Aβ amyloid (PDB ID: 2MPZ) [41]. However, methionine is not always advantageous for stable hydrophobic core formation, as demonstrated in the tentative $PrP_{107\text{-}143}$ amyloid. In terms of C_β-branching and the length of side chains, valine and methionine can cause mutually different influences on β-arches and, if the β-arch constitutes an interface between substrate monomer and template amyloid, the differences cause species/strain barriers. The influences of an M/V129 polymorphism of human PrP on the phenotypes of prion diseases and susceptibilities to certain prion strains, *e.g.*, new-variant CJD [7, 8], might be explainable from this view.

2.9. Limitation to the present method

A caveat to our view is the artificial setting, which starts with the same initial conformations irrespective of mutant types and unleashes them to move. In reality, higher freedom of motion of the backbone and potential steric effects of the long side-chain of methionine could hamper its settling into amyloid conformations. For example, spontaneous amyloid formation caused by the Y145Stop mutant of Syrian-hamster PrP, which has more methionine than the mouse or human PrP counterparts, is inefficient [21]. Such inefficiency in folding into a conformation may divert a certain fraction of molecules to aberrant refolding pathways in *in vitro* or *in vivo* experiments. Regardless of the limitations, MD simulation provides a direct insight into the structures and dynamics of in-register parallel β-sheet amyloids, and this approach can shed light on the mechanisms of strain diversity of amyloids, including PrP^{Sc}.

2.10. Conclusion

We have demonstrated how different hydrophobic amino acids uniquely affects the stability of U-shaped β-arches and consequently the entire amyloid in the two different in-register parallel β-sheet amyloids. Our studies have also revealed how the manifestation of the effects of one mutation is affected by another mutation. The notion would be applicable to various in-register parallel β-sheet amyloids and other β-arches of PrP^{Sc}. We expect that the knowledge from the present study will aid in designing more plausible PrP^{Sc} models and other amyloids in the future and advance our understanding of in-register parallel β-sheet amyloids.

3. Materials and methods

Detailed protocols of the modeling mutant αSyn amyloids, MD simulation, short MD simulation, and various analyses are mostly the same as described in the preprint on bioRxiv [25]. Here, we briefly describe the essential points.

3.1. Modeling structures of αSyn amyloids

We used a Greek-key αSyn amyloid (PDB ID: 2N0A [29]) as a starting structure, after truncating the disordered N- and C-terminal-side regions (residues 1–35 and 100–140, respectively) [25]. The N- and C-termini were acetylated and N-methylated using AmberTools16, respectively [42]. For modeling the αSyn mutants, we used SCWRL4 [43]. The modeled amyloids were solvated with a rhombic dodecahedron water box with a minimum wall distance of 12 Å using GROMACS (version 5.0.4). Na^+ and Cl^- ions were randomly placed to neutralize the system and yield a net concentration of 150 mM NaCl. The protonation state of the histidine at residue 50 was fixed as the N_δ-H tautomer (HID form in AMBER naming convention) in all simulations.

3.2. MD simulation of the αSyn amyloids

GROMACS (versions 5.0.4 and 5.1.2) [44] with the AMBER ff99SB-ILDN force field [45] was used for MD simulations with the TIP3P water model [46]. The system was initially minimized for 5,000 steps with the steepest descent method, followed by 2,000 steps with the conjugate gradient method. During minimization, heavy atoms of the amyloids were restrained with a harmonic potential with a force constant of 10.0 $\mathrm{kcal/mol \cdot Å^2}$. After minimization, the system temperature was increased from 0 to 310 K during a 1 ns simulation with the restraints. Next, a 1 ns equilibration run was performed with gradually removing the restraints from 10.0 $\mathrm{kcal/mol \cdot Å^2}$ to zero, and subsequent equilibration was performed in the NPT ensemble for 2 ns at 310 K and 1 bar. The production runs were carried out for 400 ns in the NPT ensemble at 310 K and 1 bar (Figure S3A). We used the velocity-rescaling scheme [47] and the Berendsen scheme [48] for the thermostat and barostat, respectively. The LINCS algorithm [49] was used to constrain all bonds with hydrogen atoms, allowing the use of a 2 fs time-step. Electrostatic interactions were calculated with the Particle-mesh Ewald method [50]. The cutoff length was set to 12 Å for the Coulomb and van der Waals interactions. The Verlet cutoff scheme [51] was used for neighbor-searching. Trajectory snapshots were saved every 10 ps.

3.3. Analyses

For the analyses of 400-ns simulations, the first 100 ns of each MD trajectory was discarded, and 30,001 snapshots (trajectory from 100 to 400 ns) were used. The secondary structure content during the simulations was calculated with DSSP [52, 53] using *gmx do_dssp* in GROMACS. Hydrophobic contacts were analyzed using PyInteraph [54]. A hydrophobic contact was assigned if the distance between the centers of mass of the side chains is less than 5 Å [54, 55]. The results of hydrophobic contact analyses were visualized using Cytoscape (version 3.5.1) [56]. All molecular structures for the αSyn amyloids were drawn with UCSF Chimera (version 1.12) [57] or VMD [58]. Movies of the MD simulation trajectories were prepared with UCSF Chimera [57].

3.4. Modeling $PrP_{107\text{-}143}$ amyloids and MD simulations

In designing the local structural models of human PrP^{Sc}, we adopted the region comprising $-GGL_{125}GG-$, as denoted above (see Section 2.2), and avoided charged residues in the N- and C-termini of the peptide because they can excessively destabilize in-register parallel β-sheet structures, particularly when they are at the free ends. There are positive- and negative-charge clusters in regions 101–106 and 144–147, respectively; thus, the region between them was used for the modeling. First, we roughly designed conformations of a single layer of amyloid with Swiss PDB viewer [59], then piled it up to make an in-register parallel β-sheet amyloid with UCSF Chimera [57]. The model amyloids with 10 layers were refined using Modeller (version 9.15) [60] with β-sheet restraints for the residues A120–V122, Y128–L130, and I138–F141. Mutants were generated by using SCWRL4 [43], and subsequently the N- and C-termini of the refined models were acetylated and N-methylated using PyMOL, respectively [61]. We performed 10 independent 10-ns MD simulations for each model using nearly the same procedure as the 400-ns MD simulations

of αSyn (Figure S3B). The trajectories of the production runs (0–10 ns) were analyzed as described in the *Analyses* section (see Section 3.3).

3.5. Statistical analyses

Tukey's multiple comparison test ($\alpha = 0.05$) was applied for the statistical analysis with the aid of *multcomp* package in R [62]. The graphs of the statistical analysis were drawn with *ggplot2* R package [63].

Conflict of interest

The authors declare no conflict of interest.

Author Contributions

Conceptualization, Y.T.; Methodology, H.O.; Software, H.O.; Validation, Y.T. and N.N.; Formal Analysis, Y.T. and H.O.; Investigation, H.O. and Y.T.; Resources, H.O. and N.N.; Data Curation, H.O. and Y.T.; Writing (Original Draft Preparation), Y.T.; Writing (Review & Editing), Y.T., H.O., and N.N.; Visualization, H.O. and Y.T.; Supervision, N.N.; Project Administration, Y.T.; Funding Acquisition, H.O., Y.T., and N.N.

Acknowledgements

The numerical calculations were performed on the TSUBAME2.5/3.0 supercomputer at the Tokyo Institute of Technology and the Reedbush supercomputers at the Information Technology Center, the University of Tokyo. HO acknowledges the supports of "TSUBAME Encouragement Program for Young/Female Users" of Global Scientific Information and Computing Center at the Tokyo Institute of Technology; and the "Initiative on Promotion of Supercomputing for Young or Women Researchers" of the Information Technology Center, the University of Tokyo. This work was supported by Takeda Science Foundation (www.takeda-sci.or.jp/) (to YT), and JSPS KAKENHI Grant Numbers 19K16058 (to HO) and 19K22539 (to YT).

4. Supplementary data

Supplementary data associated with this article can be found, in the online version, at *****

- Movie S1: A trajectory of MD simulation of αSyn(G84M). Only the residues 82 to 91 are shown. The side-chains of M84 and A89 are shown with sticks.
- Movie S2: A trajectory of MD simulation of $PrP_{107\text{-}143}$(WT).
- Movie S3: A trajectory of MD simulation of $PrP_{107\text{-}143}$(G127V).

References

[1] S. B. Prusiner, "Prions," *Proc. Natl. Acad. Sci. U. S. A.*, vol. 95, pp. 13 363–13 383, 1998.

[2] J. Hope, L. J. D. Reekie, N. Hunter, G. Multhaup, K. Beyreuther, H. White, A. C. Scott, M. J. Stack, M. Dawson, and G. A. H. Wells, "Fibrils from brains of cows with new cattle disease contain scrapie-associated protein," *Nature*, vol. 336, pp. 390–392, 1988.

[3] E. S. Williams, "Chronic wasting disease," *Vet. Pathol.*, vol. 42, pp. 530–549, 2005.

[4] G. C. Telling, P. Parchi, S. J. DeArmond, P. Cortelli, P. Montagna, R. Gabizon, J. Mastrianni, E. Lugaresi, P. Gambetti, and S. B. Prusiner, "Evidence for the conformation of the pathologic isoform of the prion protein enciphering and propagating prion diversity," *Science*, vol. 274, pp. 2079–2082, 1996.

[5] P. Parchi, A. Giese, S. Capellari, P. Brown, W. Schulz-Schaeffer, O. Windl, I. Zerr, H. Budka, N. Kopp, P. Piccardo, S. Poser, A. Rojiani, N. Streichemberger, J. Julien, C. Vital, B. Ghetti, P. Gambetti, and H. Kretzschmar, "Classification of sporadic Creutzfeldt-Jakob disease based on molecular and phenotypic analysis of 300 subjects," *Ann. Neurol.*, vol. 46, pp. 224–233, 1999.

[6] L. G. Goldfarb, R. B. Petersen, M. Tabaton, P. Brown, A. C. LeBlanc, P. Montagna, P. Cortelli, J. Julien, C. Vital, and W. W. Pendelbury, "Fatal familial insomnia and familial Creutzfeldt-Jakob disease: disease phenotype determined by a DNA polymorphism," *Science*, vol. 258, pp. 806–808, 1992.

[7] J. Collinge, J. Beck, T. Campbell, K. Estibeiro, and R. G. Will, "Prion protein gene analysis in new variant cases of Creutzfeldt-Jakob disease," *Lancet*, vol. 348, p. 56, 1996.

[8] J. Collinge, "Molecular neurology of prion disease," *J. Neurol. Neurosurg. Psychiatry*, vol. 76, pp. 906–919, 2005.

[9] K. M. Green, S. R. Browning, T. S. Seward, J. E. Jewell, D. L. Ross, M. A. Green, E. S. Williams, E. A. Hoover, and G. C. Telling, "The elk PRNP codon 132 polymorphism controls cervid and scrapie prion propagation," *J. Gen. Virol.*, vol. 89, pp. 598–608, 2008.

[10] A. N. Hamir, T. Gidlewski, T. R. Spraker, J. M. Miller, L. Creekmore, M. Crocheck, T. Cline, and K. I. O'Rourke, "Preliminary observations of genetic susceptibility of elk (Cervus elaphus nelsoni) to chronic wasting disease by experimental oral inoculation," *J. Vet. Diagn. Invest.*, vol. 18, pp. 110–114, 2006.

[11] E. Vázquez-Fernández, M. R. Vos, P. Afanasyev, L. Cebey, A. M. Sevillano, E. Vidal, I. Rosa, L. Renault, A. Ramos, P. J. Peters, J. J. Fernández, M. van Heel, H. S. Young, J. R. Requena, and H. Wille, "The structural architecture of an infectious mammalian prion using electron cryomicroscopy," *PLoS Pathog.*, vol. 12, p. e1005835, 2016.

[12] C. J. Silva, E. Vázquez-Fernández, B. Onisko, and J. R. Requena, "Proteinase K and the structure of PrPSc: The good, the bad and the ugly," *Virus Res.*, vol. 207, pp. 120–126, 2015.

[13] R. Tycko, R. Savtchenko, V. G. Ostapchenko, N. Makarava, and I. V. Baskakov, "The α-helical C-terminal domain of full-length recombinant PrP converts to an in-register parallel β-sheet structure in PrP fibrils: Evidence from solid state nuclear magnetic resonance," *Biochemistry*, vol. 49, pp. 9488–9497, 2010.

[14] B. R. Groveman, M. A. Dolan, L. M. Taubner, A. Kraus, R. B. Wickner, and B. Caughey, "Parallel in-register intermolecular β-sheet architectures for prion-seeded prion protein (PrP) amyloids," *J. Biol. Chem.*, vol. 289, pp. 24 129–24 142, 2014.

[15] N. J. Cobb, F. D. Sönnichsen, H. Mchaourab, and W. K. Surewicz, "Molecular architecture of human prion protein amyloid: A parallel, in-register β-structure," *Proc. Natl. Acad. Sci. U. S. A.*, vol. 104, pp. 18 946–18 951, 2007.

[16] T. Theint, Y. Xia, P. S. Nadaud, D. Mukhopadhyay, C. D. Schwieters, K. Surewicz, W. K. Surewicz, and C. P. Jaroniec, "Structural studies of amyloid fibrils by paramagnetic solid-state nuclear magnetic resonance spectroscopy," *J. Am. Chem. Soc.*, vol. 140, pp. 13 161–13 166, 2018.

[17] S. A. Priola and B. Chesebro, "A single hamster PrP amino acid blocks conversion to protease-resistant PrP in scrapie-infected mouse neuroblastoma cells," *J. Virol.*, vol. 69, pp. 7754–7758, 1995.

[18] D. L. Vanik, K. A. Surewicz, and W. K. Surewicz, "Molecular basis of barriers for interspecies transmissibility of mammalian prions," *Mol. Cell*, vol. 14, pp. 139–145, 2004.

[19] K. Giles, G. F. De Nicola, S. Patel, D. V. Glidden, C. Korth, A. Oehler, S. J. DeArmond, and S. B. Prusiner, "Identification of I137M and other mutations that modulate incubation periods for two human prion strains," *J. Virol.*, vol. 86, pp. 6033–6041, 2012.

[20] D. H. Lowenstein, D. A. Butler, D. Westaway, M. P. McKinley, S. J. DeArmond, and S. B. Prusiner, "Three hamster species with different scrapie incubation times and neuropathological features encode distinct prion proteins," *Mol. Cell. Biol.*, vol. 10, pp. 1153–1163, 1990.

[21] K. D. Meade-White, K. D. Barbian, B. Race, C. Favara, D. Gardner, L. Taubner, S. Porcella, and R. Race, "Characteristics of 263K scrapie agent in multiple hamster species," *Emerging Infect. Dis.*, vol. 15, pp. 207–215, 2009.

[22] T. Shirai, M. Saito, A. Kobayashi, M. Asano, M. Hizume, S. Ikeda, K. Teruya, M. Morita, and T. Kitamoto, "Evaluating prion models based on comprehensive mutation data of mouse PrP," *Structure*, vol. 22, pp. 560–571, 2014.

[23] C. Harrathi, N. Fernández-Borges, H. Eraña, S. R. Elezgarai, V. Venegas, J. M. Charco, and J. Castilla, "Insights into the bidirectional properties of the sheep - deer prion transmission barrier," *Mol. Neurobiol.*, vol. 56, pp. 5287–5303, 2019.

[24] Y. Taguchi, H. Otaki, and N. Nishida, "Mechanisms of strain diversity of disease-associated in-register parallel β-sheet amyloids and implications about prion strains," *Viruses*, vol. 11, p. 110, 2019.

[25] H. Otaki, Y. Taguchi, and N. Nishida, "Molecular dynamics simulation reveals that switchable combinations of β-sheets underlie the prion-like properties of α-synuclein amyloids," *bioRxiv*, vol. 326462, 2018.

[26] R. Melki, "Alpha-synuclein and the prion hypothesis in Parkinson's disease," *Rev. Neurol. (Paris)*, vol. 174, pp. 644–652, 2018.

[27] L. Bousset, L. Pieri, G. Ruiz-Arlandis, J. Gath, P. H. Jensen, B. Habenstein, K. Madiona, V. Olieric, A. Böckmann, B. H. Meier, and R. Melki, "Structural and functional characterization of two alpha-synuclein strains," *Nat. Commun.*, vol. 4, p. 2575, 2013.

[28] C. Peng, R. J. Gathagan, D. J. Covell, C. Medellin, A. Stieber, J. L. Robinson, B. Zhang, R. M. Pitkin, M. F. Olufemi, K. C. Luk, J. Q. Trojanowski, and V. M. Y. Lee, "Cellular milieu imparts distinct pathological α-synuclein strains in α-synucleinopathies," *Nature*, vol. 557, pp. 558–563, 2018.

[29] M. D. Tuttle, G. Comellas, A. J. Nieuwkoop, D. J. Covell, D. A. Berthold, K. D. Kloepper, J. M. Courtney, J. K. Kim, A. M. Barclay, A. Kendall, W. Wan, G. Stubbs, C. D. Schwieters, V. M. Y. Lee, J. M. George, and C. M. Rienstra, "Solid-state NMR structure of a pathogenic fibril of full-length human α-synuclein," *Nat. Struct. Mol. Biol.*, vol. 23, pp. 409–415, 2016.

[30] B. Li, P. Ge, K. A. Murray, P. Sheth, M. Zhang, G. Nair, M. R. Sawaya, W. S. Shin, D. R. Boyer, S. Ye, D. S. Eisenberg, Z. H. Zhou, and L. Jiang, "Cryo-EM of full-length α-synuclein reveals fibril polymorphs with a common structural kernel," *Nat. Commun.*, vol. 9, p. 3609, 2018.

[31] R. Guerrero-Ferreira, N. M. I. Taylor, D. Mona, P. Ringler, M. E. Lauer, R. Riek, M. Britschgi, and H. Stahlberg, "Cryo-EM structure of alpha-synuclein fibrils," *eLife*, vol. 7, p. e36402, 2018.

[32] E. A. Asante, M. Smidak, A. Grimshaw, R. Houghton, A. Tomlinson, A. Jeelani, T. Jakubcova, S. Hamdan, A. Richard-Londt, J. M. Linehan, S. Brandner, M. Alpers, J. Whitfield, S. Mead, J. D. F. Wadsworth, and J. Collinge, "A naturally occurring variant of the human prion protein completely prevents prion disease," *Nature*, vol. 522, pp. 478–481, 2015.

[33] T. Theint, P. S. Nadaud, D. Aucoin, J. J. Helmus, S. P. Pondaven, K. Surewicz, W. K. Surewicz, and C. P. Jaroniec, "Species-dependent structural polymorphism of Y145Stop prion protein amyloid revealed by solid-state NMR spectroscopy," *Nat. Commun.*, vol. 8, p. 753, 2017.

[34] J.-K. Choi, I. Cali, K. Surewicz, Q. Kong, P. Gambetti, and W. K. Surewicz, "Amyloid fibrils from the N-terminal prion protein fragment are infectious," *Proc. Natl. Acad. Sci. U. S. A.*, vol. 113, pp. 13 851–13 856, 2016.

[35] P. C. Lyu, J. C. Sherman, A. Chen, and N. R. Kallenbach, "α-Helix stabilization by natural and unnatural amino acids with alkyl side chains," *Proc. Natl. Acad. Sci. U. S. A.*, vol. 88, pp. 5317–5320, 1991.

[36] J. M. Berg, J. L. Tymoczko, and L. Stryer, "The amino acid sequence of a protein determines its three-dimensional structure," in *Biochemistry*, 5th ed. New York: W H Freeman, 2002.

[37] W. Goldmann, N. Hunter, G. Smith, J. Foster, and J. Hope, "PrP genotype and agent effects in scrapie: Change in allelic interaction with different isolates of agent in sheep, a natural host of scrapie," *J. Gen. Virol.*, vol. 75, pp. 989–995, 1994.

[38] B. R. Groveman, G. J. Raymond, K. J. Campbell, B. Race, L. D. Raymond, A. G. Hughson, C. D. Orrú, A. Kraus, K. Phillips, and B. Caughey, "Role of the central lysine cluster and scrapie templating in the transmissibility of synthetic prion protein aggregates," *PLoS Pathog.*, vol. 13, p. e1006623, 2017.

[39] Y. Taguchi, A. M. A. Mistica, T. Kitamoto, and H. M. Schätzl, "Critical significance of the region between helix 1 and 2 for efficient

dominant-negative inhibition by conversion-incompetent prion protein," *PLoS Pathog.*, vol. 9, p. e1003466, 2013.

[40] Y. Taguchi, L. Lu, C. Marrero-Winkens, H. Otaki, N. Nishida, and H. M. Schatzl, "Disulfide-crosslink scanning reveals prion-induced conformational changes and prion strain-specific structures of the pathological prion protein PrP^{Sc}," *J. Biol. Chem.*, vol. 293, pp. 12 730–12 740, 2018; ——, "Correction: Disulfide-crosslink scanning reveals prion-induced conformational changes and prion strain-specific structures of the pathological prion protein PrP^{Sc}," *J. Biol. Chem.*, vol. 293, p. 14925, 2018.

[41] N. Sgourakis, W.-M. Yau, and W. Qiang, "Modeling an in-register, parallel "iowa" Aβ fibril structure using solid-state NMR data from labeled samples with Rosetta," *Structure*, vol. 23, pp. 216–227, 2015.

[42] D. Case, R. Betz, D. Cerutti, I. T. Cheatham, T. Darden, R. Duke, T. Giese, H. Gohlke, A. Goetz, N. Homeyer, S. Izadi, P. Janowski, J. Kaus, A. Kovalenko, T. Lee, S. LeGrand, P. Li, C. Lin, T. Luchko, R. Luo, B. Madej, D. Mermelstein, K. Merz, G. Monard, H. Nguyen, H. Nguyen, I. Omelyan, A. Onufriev, D. Roe, A. Roitberg, C. Sagui, C. Simmerling, W. Botello-Smith, J. Swails, R. Walker, J. Wang, R. Wolf, X. Wu, L. Xiao, and P. Kollman, "AmberTools16," 2016.

[43] G. G. Krivov, M. V. Shapovalov, and R. L. Dunbrack, "Improved prediction of protein side-chain conformations with SCWRL4," *Proteins: Struct. Funct. Bioinform.*, vol. 77, pp. 778–795, 2009.

[44] M. J. Abraham, T. Murtola, R. Schulz, S. Páll, J. C. Smith, B. Hess, and E. Lindahl, "GROMACS: High performance molecular simulations through multi-level parallelism from laptops to supercomputers," *SoftwareX*, vol. 1-2, pp. 19–25, 2015.

[45] K. Lindorff-Larsen, S. Piana, K. Palmo, P. Maragakis, J. L. Klepeis, R. O. Dror, and D. E. Shaw, "Improved side-chain torsion potentials for the amber ff99SB protein force field," *Proteins: Struct. Funct. Bioinform.*, vol. 78, pp. 1950–1958, 2010.

[46] W. L. Jorgensen, J. Chandrasekhar, J. D. Madura, R. W. Impey, and M. L. Klein, "Comparison of simple potential functions for simulating liquid water," *J. Chem. Phys.*, vol. 79, pp. 926–935, 1983.

[47] G. Bussi, D. Donadio, and M. Parrinello, "Canonical sampling through velocity rescaling," *J. Chem. Phys.*, vol. 126, p. 014101, 2007.

[48] H. J. C. Berendsen, J. P. M. Postma, W. F. van Gunsteren, A. DiNola, and J. R. Haak, "Molecular dynamics with coupling to an external bath," *J. Chem. Phys.*, vol. 81, pp. 3684–3690, 1984.

[49] B. Hess, "P-LINCS: A parallel linear constraint solver for molecular simulation," *J. Chem. Theory Comput.*, vol. 4, pp. 116–122, 2008.

[50] U. Essmann, L. Perera, M. L. Berkowitz, T. Darden, H. Lee, and L. G. Pedersen, "A smooth particle mesh Ewald method," *J. Chem. Phys.*, vol. 103, pp. 8577–8593, 1995.

[51] S. Páll and B. Hess, "A flexible algorithm for calculating pair interactions on SIMD architectures," *Comput. Phys. Commun.*, vol. 184, pp. 2641–2650, 2013.

[52] W. G. Touw, C. Baakman, J. Black, T. A. H. te Beek, E. Krieger, R. P. Joosten, and G. Vriend, "A series of PDB-related databanks for everyday needs," *Nucleic Acids Res.*, vol. 43, pp. D364–D368, 2015.

[53] W. Kabsch and C. Sander, "Dictionary of protein secondary structure: Pattern recognition of hydrogen-bonded and geometrical features," *Biopolymers*, vol. 22, pp. 2577–2637, 1983.

[54] M. Tiberti, G. Invernizzi, M. Lambrughi, Y. Inbar, G. Schreiber, and E. Papaleo, "Pyinteraph: A framework for the analysis of interaction networks in structural ensembles of proteins," *J. Chem. Inf. Model.*, vol. 54, pp. 1537–1551, 2014.

[55] J. Salamanca Viloria, M. F. Allega, M. Lambrughi, and E. Papaleo, "An optimal distance cutoff for contact-based protein structure networks using side-chain centers of mass," *Sci. Rep.*, vol. 7, p. 2838, 2017.

[56] P. Shannon, A. Markiel, O. Ozier, N. S. Baliga, J. T. Wang, D. Ramage, N. Amin, B. Schwikowski, and T. Ideker, "Cytoscape: A software environment for integrated models of biomolecular interaction networks," *Genome Res.*, vol. 13, pp. 2498–2504, 2003.

[57] E. F. Pettersen, T. D. Goddard, C. C. Huang, G. S. Couch, D. M. Greenblatt, E. C. Meng, and T. E. Ferrin, "UCSF Chimera—A visualization system for exploratory research and analysis," *J. Comput. Chem.*, vol. 25, pp. 1605–1612, 2004.

[58] W. Humphrey, A. Dalke, and K. Schulten, "VMD: Visual molecular dynamics," *J. Mol. Graphics*, vol. 14, pp. 33–38, 1996.

[59] N. Guex and M. C. Peitsch, "SWISS-MODEL and the Swiss-Pdb Viewer: An environment for comparative protein modeling," *Electrophoresis*, vol. 18, pp. 2714–2723, 1997.

[60] A. Šali and T. L. Blundell, "Comparative protein modelling by satisfaction of spatial restraints," *J. Mol. Biol.*, vol. 234, pp. 779–815, 1993.

[61] W. L. DeLano, "Pymol: An open-source molecular graphics tool," *CCP4 Newsletter On Protein Crystallography*, vol. 40, pp. 82–92, 2002.

[62] T. Hothorn, F. Bretz, and P. Westfall, "Simultaneous inference in general parametric models," *Biom. J.*, vol. 50, no. 3, pp. 346–363, 2008.

[63] H. Wickham, *ggplot2: Elegant Graphics for Data Analysis*. New York: Springer-Verlag, 2016. [Online]. Available: https://ggplot2.tidyverse.org

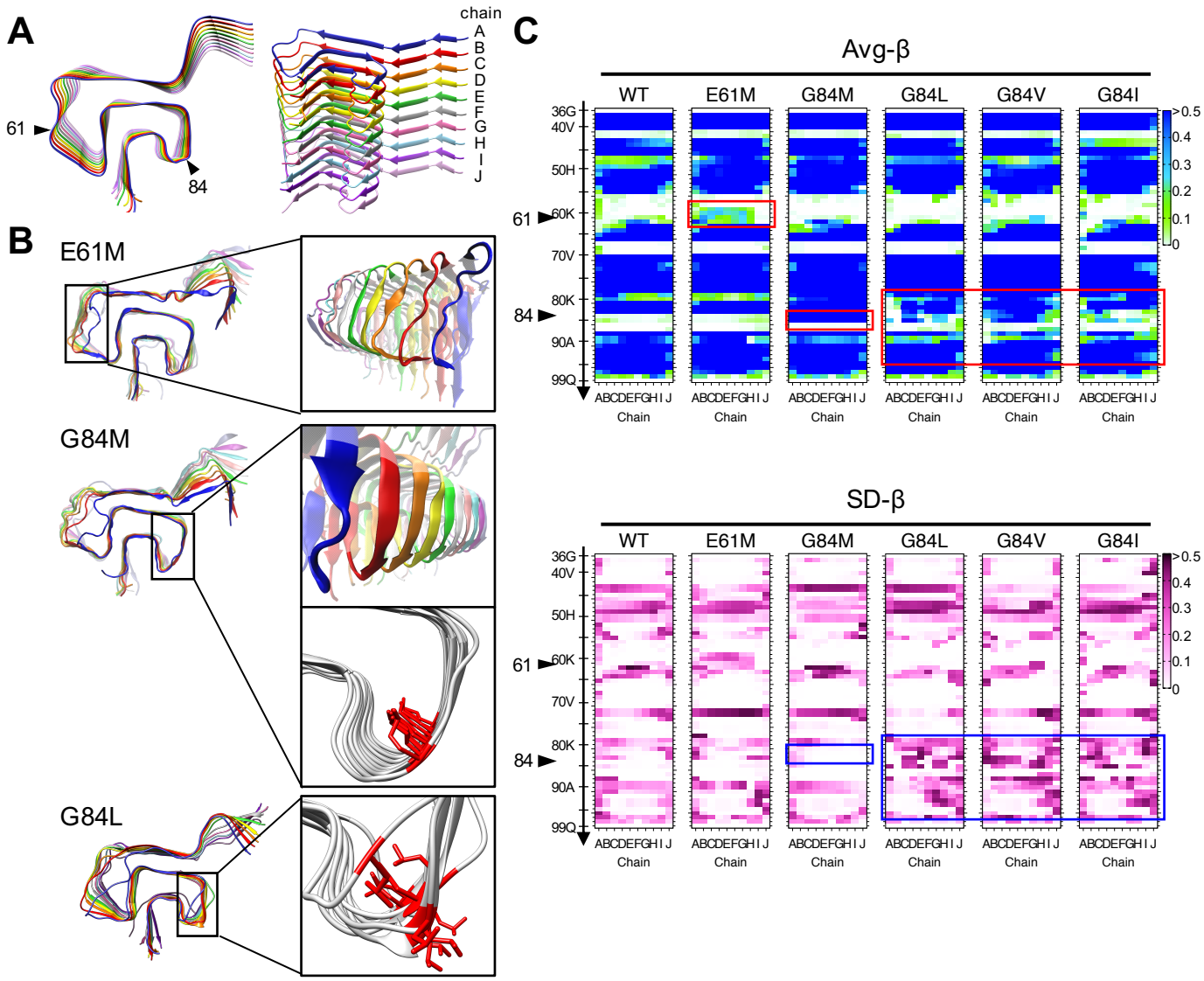

Figure 1: Influences of E61M and G84M/L/V/I substitutions on local structures of Greek-key αSyn amyloid: (A) Structure of the Greek-key αSyn amyloid (PDB ID: 2N0A), in which N- and C-terminal-side regions (residues 1–35 and 100–140, respectively) are truncated. The black triangles indicate the positions of residues 61 and 84. The chains of the amyloid stack are referred to as chains A–J. (B) Final snapshots of αSyn(E61M), αSyn(G84M), and αSyn(G84L) amyloids after 400-ns MD simulations. The insets present magnified views of the indicated regions. Note that the β-sheets are induced in loop(57–62) of the αSyn(E61M) amyloid and that the αSyn(G84M) amyloid has β-sheets extended to loop(84–87). In αSyn(G84M) and αSyn(G84L), directions of the side chains of residue 84 after a 400-ns MD simulation are shown with red sticks in the insets. In αSyn(G84L), the local structures around the mutation were disturbed. Some side chains of L84 are pointing outward, whereas those of M84 remain inside. (C) Heatmaps of the average β-sheet propensity values (Avg-β) and the standard deviation of the values (SD-β) based on five (for WT) and three (for the mutants) independent 400-ns MD simulations. The vertical axes and horizontal axes of all the heatmaps represent the residue numbers and the chains A–J, respectively. The black triangles indicate the positions of E61M and G84M. Avg-β values in loop(57–62) of αSyn(E61M) and loop(84–87) of the αSyn(G84M) amyloids increased (E61M and G84M, red boxes), corresponding to the induced β-sheets in those regions (see (A), (B)). The relatively low SD-β values in the αSyn(G84M) amyloid (G84M, blue box) reflect stablized local structures. In αSyn(G84L), αSyn(G84V), and αSyn(G84I), the structural disturbances caused by the mutation are reflected to the heatmap (G84L/V/I, red and blue boxes). The heatmaps of WT and G84I mutant are taken from Taguchi *et al.* (2019) [24] published under the CC-BY 4.0 license.

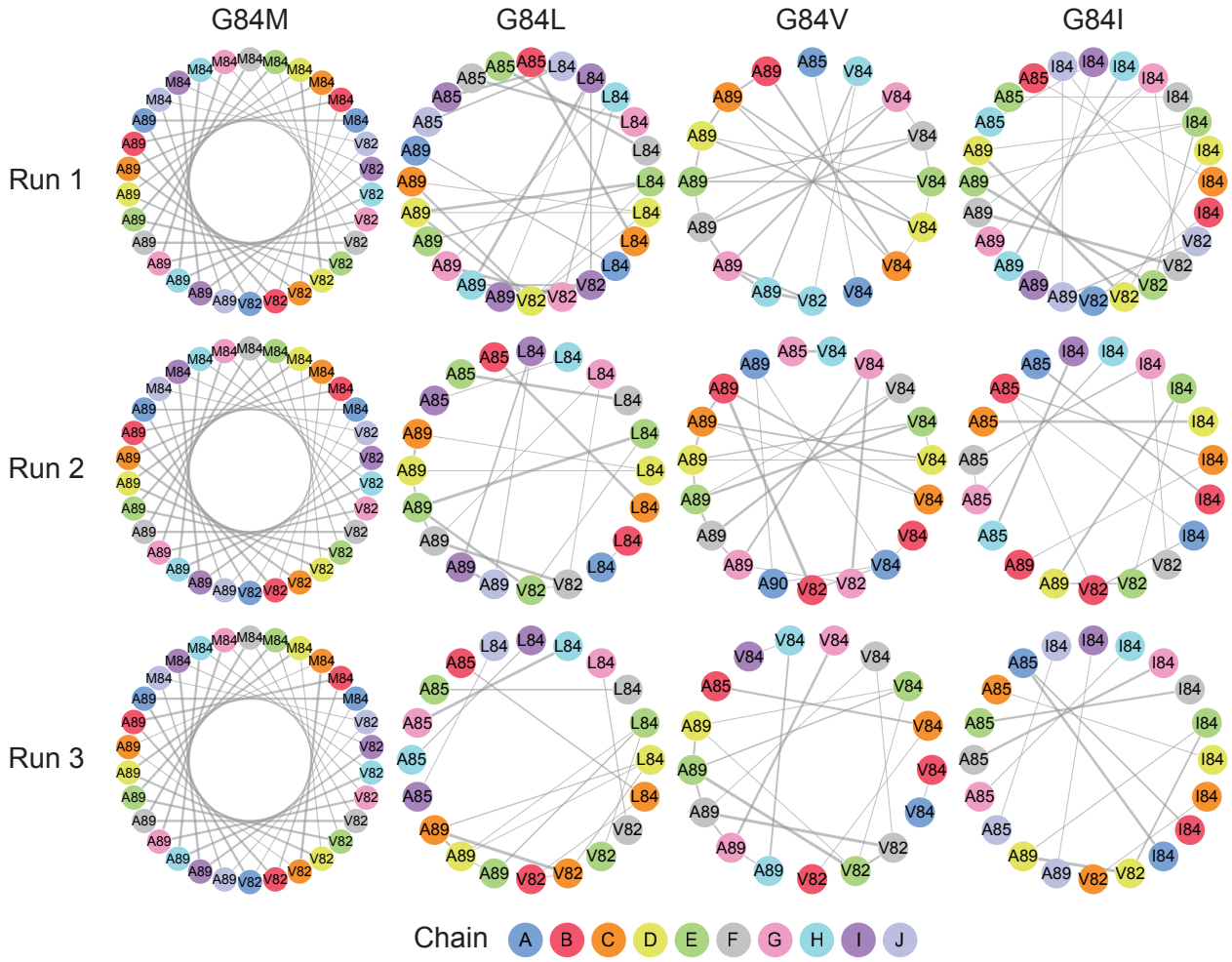

Figure 2: Hydrophobic contact diagrams based on 400-ns simulations of αSyn amyloids. Only the residues involved in the interactions with residue 84 are presented. Residue numbers and chains are indicated by numbers and colors of the dots, respectively. The thickness of each line corresponds to occupancy of the hydrophobic contact.

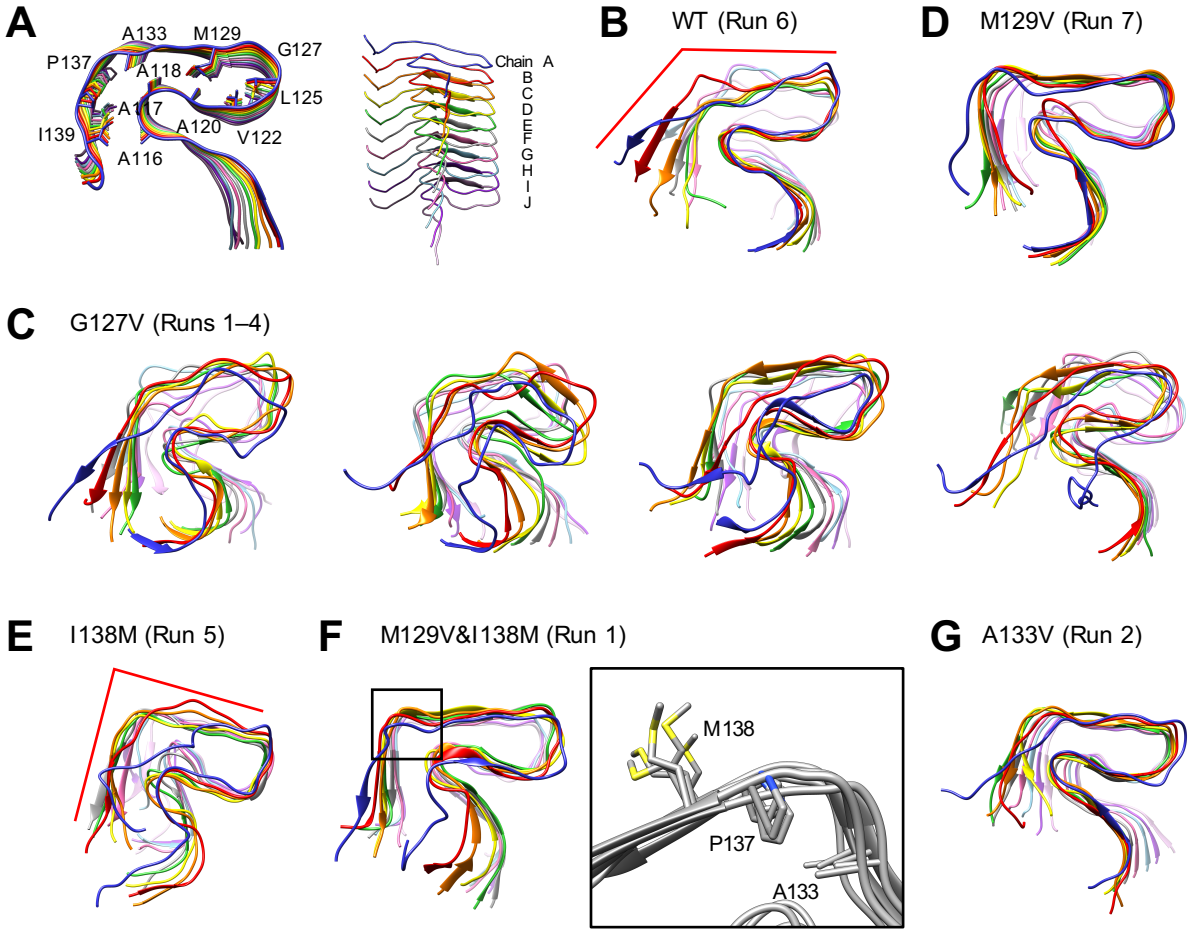

Figure 3: Local-structural model of PrP^{Sc} and final snapshots of 10-ns MD simulations. For all the snapshots of 10 runs (except for G127V), see Figure S2: (A) A $PrP_{107\text{-}143}$ amyloid as a tentative local-structural model of PrP^{Sc} and an oblique view showing the 10 layers (chains A–J). Side chains of the residues that are mentioned later are annotated. (B) A final snapshot of WT $PrP_{107\text{-}143}$ after a 10-ns MD simulation (WT, Run 6). (C) Final snapshots of $PrP_{107\text{-}143}$(G127V) in four consective runs (G127V, Run 1–4) of 10-ns MD simulations. (D) A final snapshot of $PrP_{107\text{-}143}$(M129V) after a 10-ns MD simulation (M129V, Run 7). (E) A final snapshot of $PrP_{107\text{-}143}$(I138M) after a 10-ns MD simulation (I138M, Run 5). (F) (Left) A final snapshot of $PrP_{107\text{-}143}$(M129V&I138M) after a 10-ns MD simulation (M129V&I138M, Run 1). The box indicates Ω-shaped loops encompassing A133 to P137. (Right) Positional relationships of the side chains of A133, P137, and M138 in chains B–F. (G) A final snapshot of $PrP_{107\text{-}143}$(A133V) after a 10-ns MD simulation (A133V, Run 2).

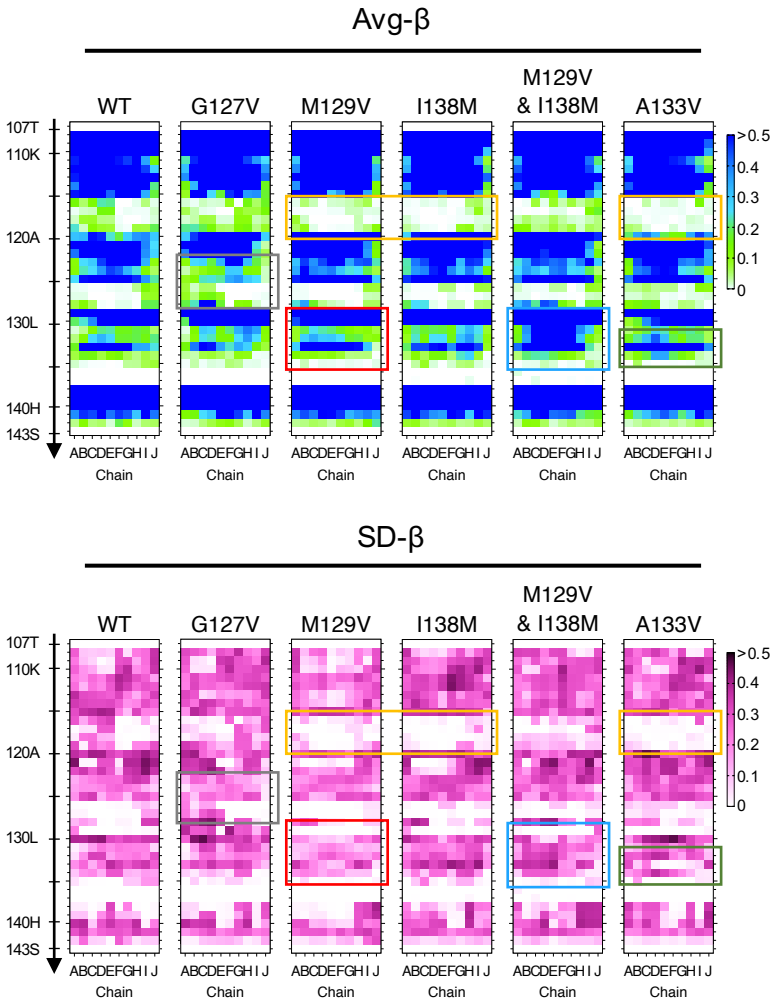

Figure 4: Heatmaps showing the Avg-β and the SD-β of each residue of the WT and the mutant $PrP_{107\text{-}143}$ amyloids (G127V, M129V, I138M, M129V&I138M, and A133V). The values were calculated from 10 independent 10-ns MD runs: Yellow boxes, more demarcated loop(116–119) than in WT; Red boxes, more stable β-sheet(128–133) with lower SD-β values than in WT; Green boxes, higher β-sheet propensity at V133 with lower SD-β values than in WT; Gray boxes, disordered loop(123–127); Blue boxes, higher β-sheet propensity at residues 131–132 and higher SD-β value at V133 induced by "upward shift" (see Figure 7E,F).

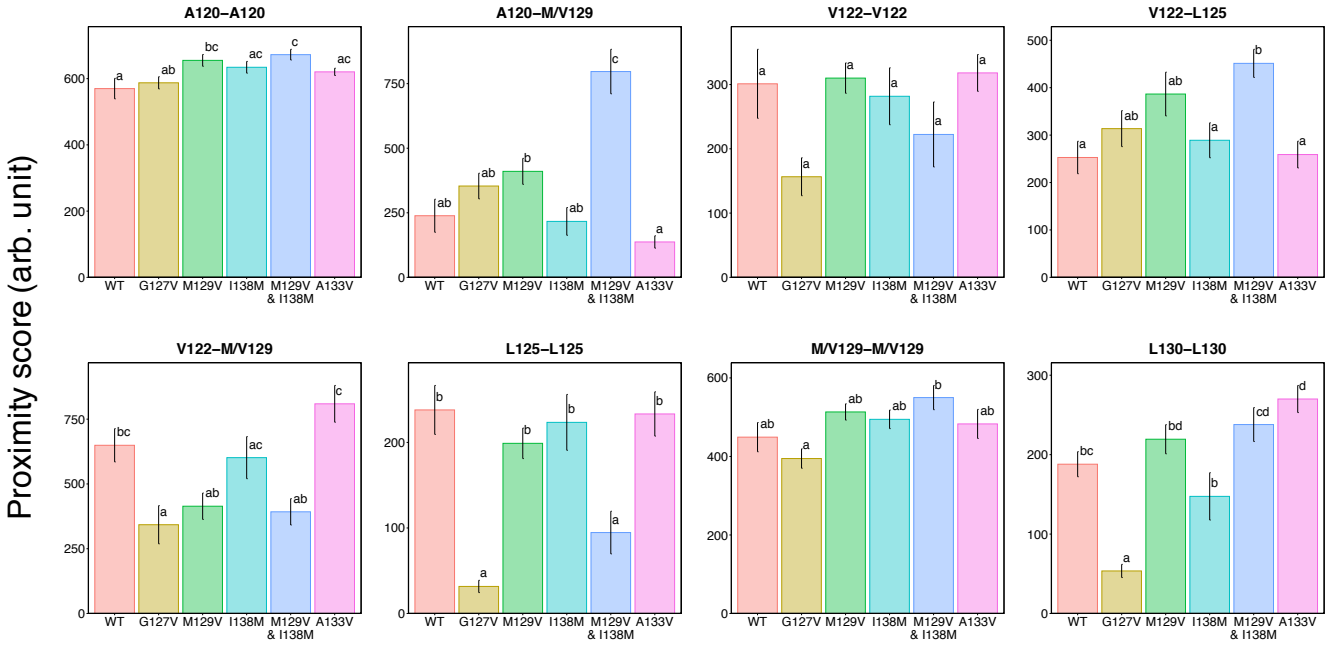

Figure 5: Bar plots of proximity scores between two residues in the U-shaped loop (residues 120–130). The error bar represents standard error (SE) of mean of values from 10 independent MD runs. Bars sharing the same letter are not significantly different according to Tukey's test with $\alpha = 0.05$.

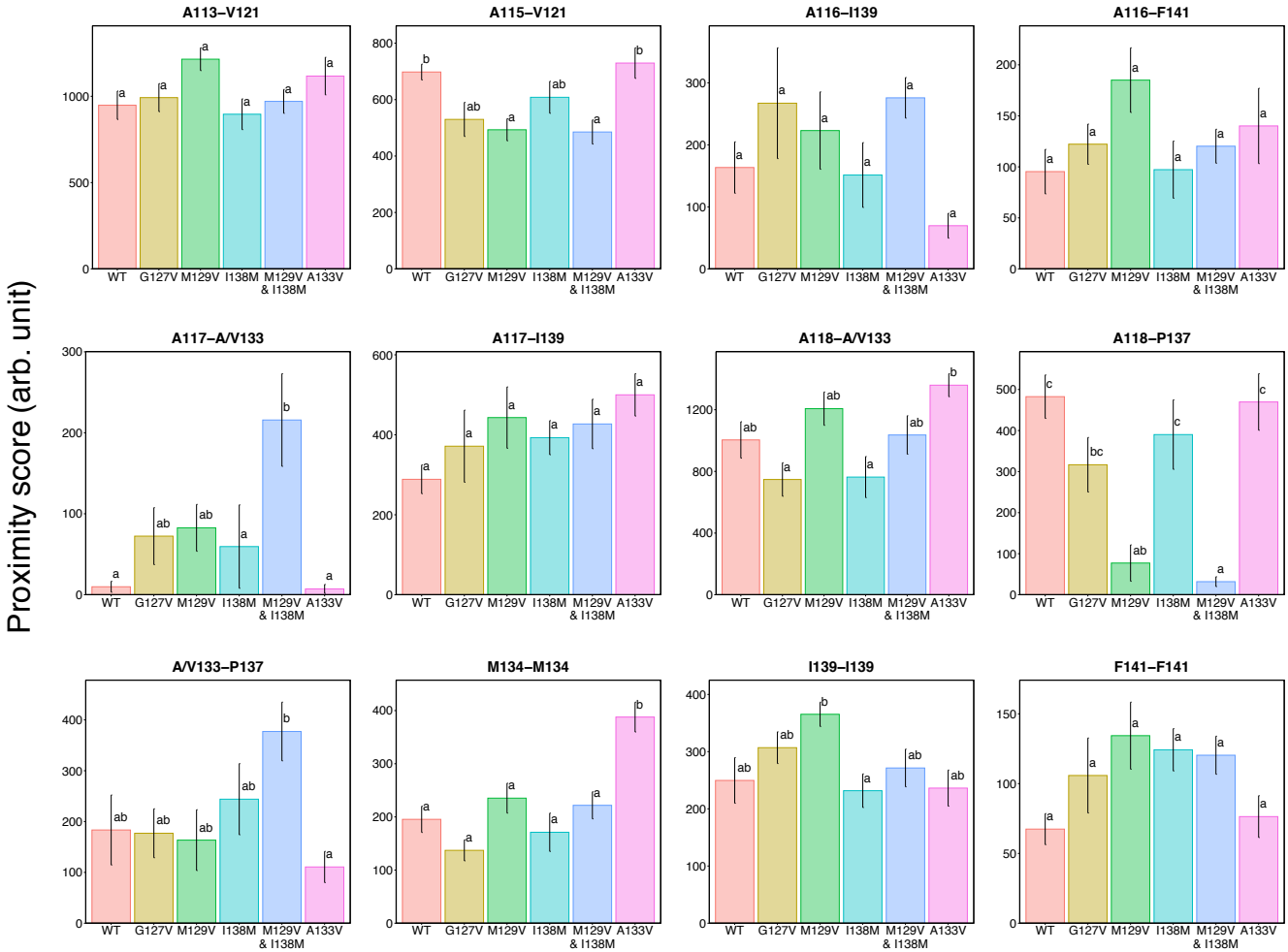

Figure 6: Same as Figure 5, but for the residues in the N- and C-terminal-side regions.

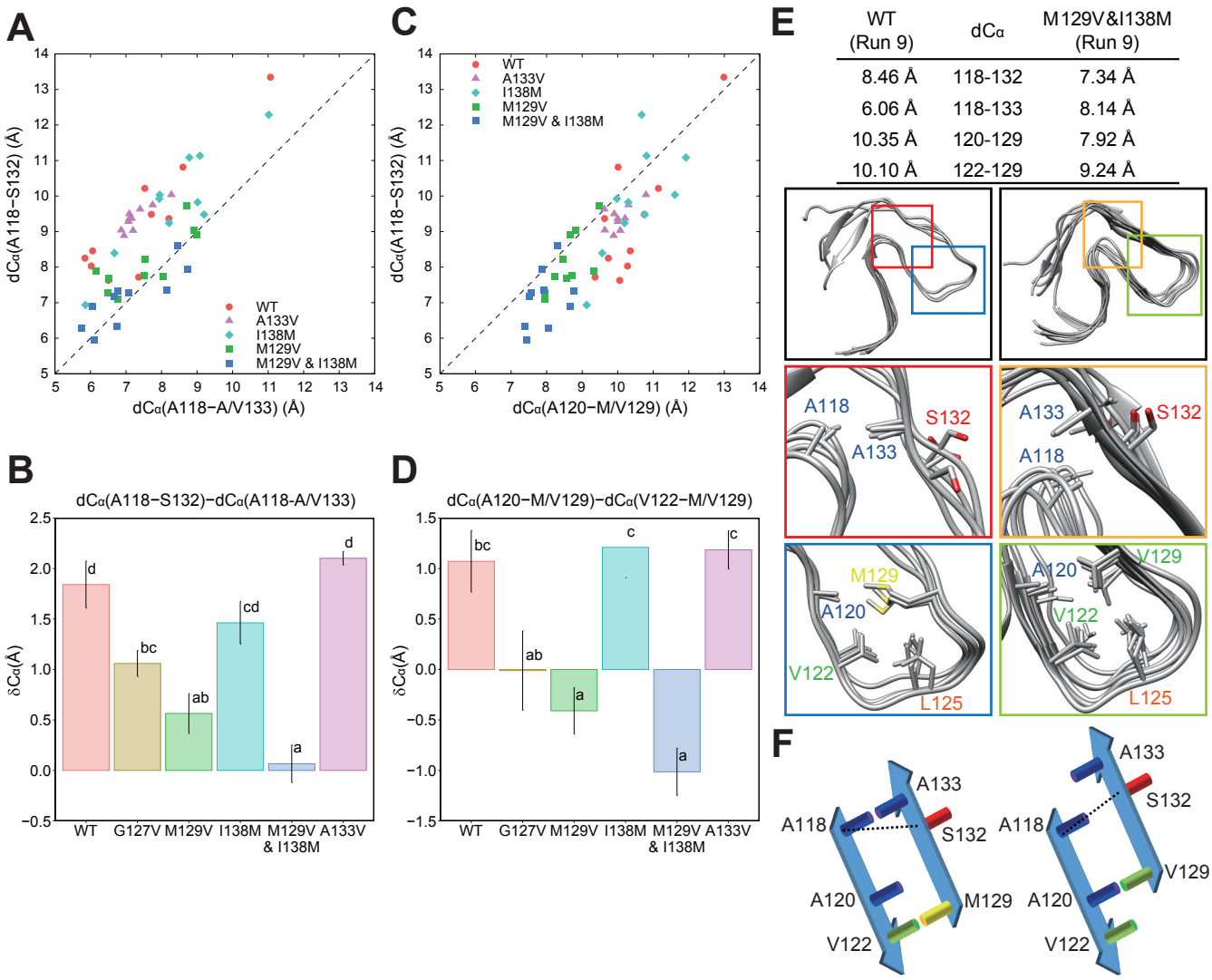

Figure 7: (A) Scatter plot showing correlations of the final C_α-C_α distances for A118-A/V133 (dC_α(A118-A/V133)) and A118-S132 (dC_α(A118-S132)) in the WT and mutant $PrP_{107\text{-}143}$ amyloids. The dashed line is merely guide to the eye. (B) Bar plot of difference between the final C_α-C_α distances, δC_α, for dC_α(A118-S132) and dC_α(A118-A/V133) in the WT and mutant $PrP_{107\text{-}143}$ amyloids. The bars and error bars represent mean ± standard error (SE) of values from 10 independent MD runs. Bars sharing the same letter are not significantly different according to Tukey's test with $\alpha = 0.05$. (C) Same as (A), but for dC_α(A120-M/V129) and dC_α(A118-S132). Note that the dC_α(A120-M/V129) values of $PrP_{107\text{-}143}$ with M129V mutations (green and blue squares) are shorter than 9 Å in most of the MD runs and their dC_α(A118-S132) values also tend to be shorter than those of the other mutants. (D) Same as (B), but for the difference between dC_α(A120-M/V129) and dC_α(V122-M/V129). (E) Final snapshots of the chains D–G of WT $PrP_{107\text{-}143}$ and chains C–H of $PrP_{107\text{-}143}$(M129V&I138M) after 10-ns MD simulations. Upper table shows the C_α-C_α distances between the residues averaged over chains A–J. The insets show magnified views with the side chains of the residues involved in hydrophobic interactions. (F) A schematic illustration of the positional relationships and "upward shift" of the β-sheet(128–133) induced by the M129V mutation. The dashed lines indicate distances between the C_α atoms of A118 and S132.

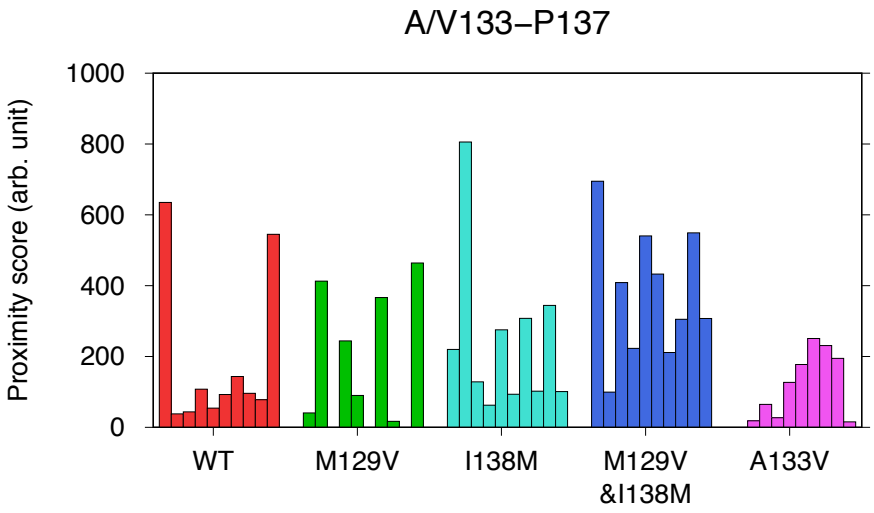

Figure 8: Proximity scores for A/V133-P137. Each bar represents the value obtained from each of the 10 runs (Run 1 to 10, from left to right).

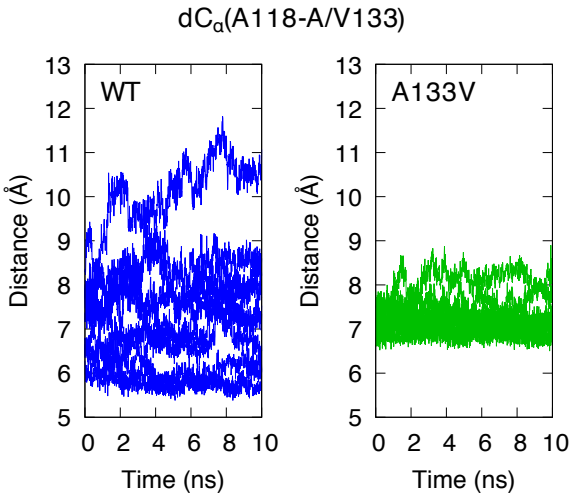

Figure 9: Fluctuations in the average distance between C_α atoms of A118 and A/V133, dC_α(A118-A/V133), over 10 ns. Each line represents the average of the distances over chains A–J in each of the 10 runs.